


Article

Tie-system calibration for the experimental setup of large deployable reflectors

A. Cammarata^{1*}, R. Sinatra¹, R. Rigato² and P.D. Maddio¹¹ University of Catania; alessandro.cammarata@unict.it; rosario.sinatra@unict.it; pietero.maddio@unict.it² Thales Alenia Space Italia; riccardo.rigato@thalesaleniaspace.com

* Correspondence: alessandro.cammarata@unict.it; Tel.: +39-095-738-2403

Version March 12, 2019 submitted to Preprints

Abstract: The tradeoff between the design phase and the experimental setup is crucial to satisfy the accuracy requirement of Large Deployable Reflectors. Manufacturing errors and tolerances change the RMS of the reflecting surface and require careful calibration of the tie rod system to be able to fit into the initial design specifications. To give a possible solution to this problem, here two calibration methods, respectively for rigid and flexible ring truss support, are described. Starting from the acquired experimental data on the net nodal coordinates, the initial problem of satisfying the static equilibrium at the measured configuration is described. Then, two constrained optimization problems, for rigid and flexible ring truss support, are defined to meet RMS accuracy of the reflecting surface modifying the tie lengths. Finally, a case study to demonstrate the validity of the proposed methods is presented.

Keywords: large deployable reflector; tie adjustment; experimental setup

1. Introduction

In recent decades, satellite communications have been increasingly spread thanks to the possibility of having high transmitting capacities at a relatively low cost compared to the establishment of a terrestrial broadcasting network. The deployable reflectors represent the most widely used type of structure because of their features such as large scale, high packaging efficiency, high accuracy and lightweight. Typically, its architecture consists of a deployable ring truss support, two cable nets, facing each other and linked by a series of tension ties, and an RF mesh attached to the backside of the front net. The most representative kind of this type of reflector is the AstroMesh [1], and its components are shown in Fig. 1. The electromagnetic performance of these antennas is closely related to the shape of the reflector surface. In turn, this depends on the position of nodes located on the front net. Therefore, it is clear how the measurement process of 3D node coordinates is to be made with extreme accuracy so as to avoid invalidating the real root mean square (RMS) value.

In recent years several measurement systems have been developed depending on the application area. Generally, they can be summarised in three categories:

- Photogrammetry
- Laser tracker
- Laser radar

The photogrammetry is a measurement technique that uses two-dimensional images of an object to obtain its dimensions. As depicted in Fig. 2 the photogrammetry is based exclusively on angle measurements: three-dimensional coordinates are calculated via optical triangulation (or *intersection*) of two or more images taken from different positions. The object to be measured is identified by targets mounted on it, usually made of reflective material so as to produce high contrast between the target and the background [2]. Typically, a calibrated scale bar is integrated into the object in order to reproduce it in true scale. At the end of measurements, a dedicated software calculates the 3D coordinates into the chosen Cartesian coordinate system (x, y, z).

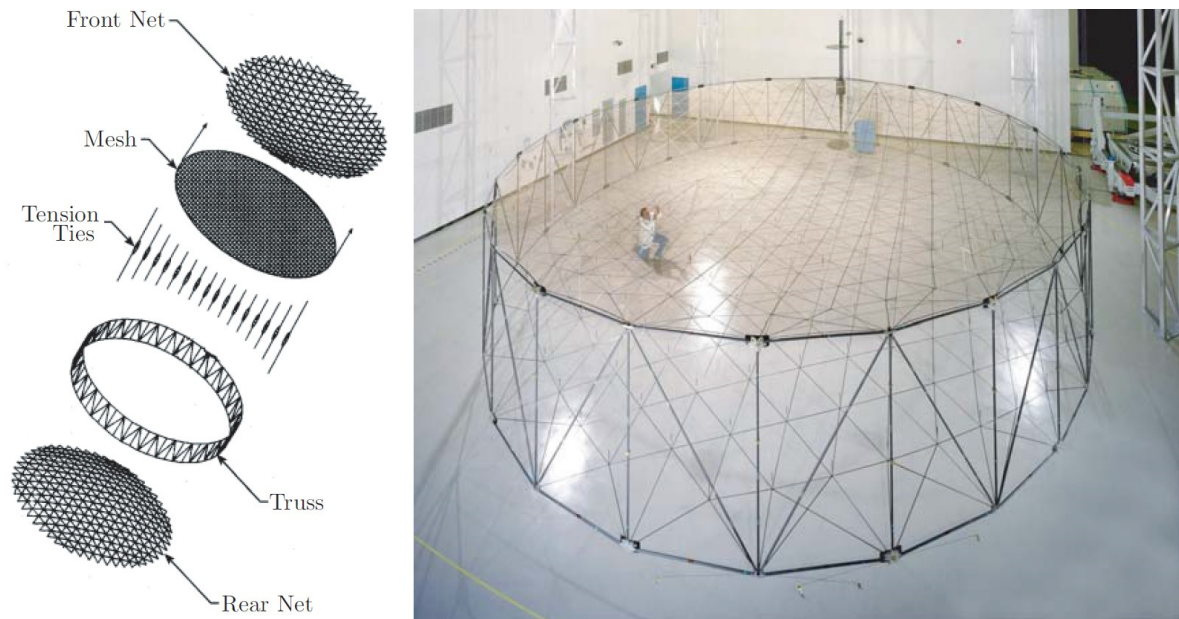


Figure 1. AstroMesh

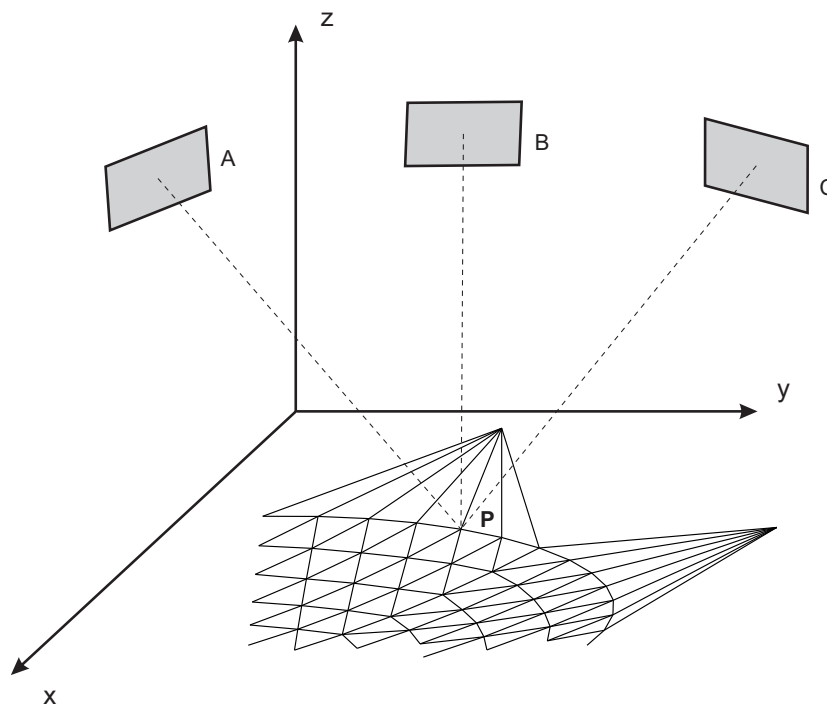


Figure 2. Photogrammetry

37 Laser tracker and laser radar, instead, are measurement systems based on the estimation of two
 38 angles and one length, as shown in Fig. 3. Two high-resolution encoders measure the azimuth (θ) and
 39 elevation (φ) angles, whereas the radial coordinate (r) relative to the center of the target is measured
 40 by means of optical interference [3]. Several types of target can be mounted, but the most widely used
 41 is the spherically mounted retroreflector (SMR). Differently from laser tracker, laser radar does not
 42 require a retroreflector. As a matter of fact, it is capable of measuring the surface of the object with just
 43 1% of the reflected signal [4].

44 Each of these measurement systems, however, has advantages and disadvantages, which need
 45 to be assessed on the basis of various factors. Van Gestel *et al.* [4] identify the influencing factors to
 46 be taken into account before making the measurement, i.e.: task requirements, part restrictions and

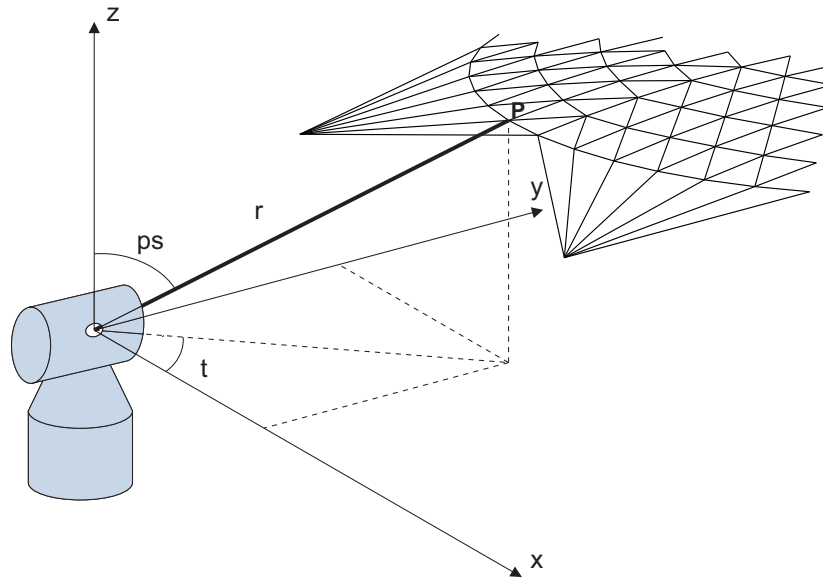


Figure 3. Laser tracker

47 environmental restrictions. Regarding task requirements, the main element to be considered when
 48 measuring the position of nodes is the accuracy, since the permissible RMS error on the reflecting
 49 surface is less than 1 (mm). Whilst the laser tracker has errors on the order of $1 \mu\text{m}$, it is too costly due to
 50 the high price of each SMR and given the number of nodes (at least a hundred). The photogrammetry
 51 turns out to be the best choice [5,6], considering the affordable cost and accuracy of the measure.
 52 Furthermore, the possibility of obtaining multiple images from different angles makes it possible to
 53 overcome the lower accuracy of the angular encoders of laser trackers.

54 The acquisition of node coordinates is essential for the next calibration step in order to meet the
 55 RMS design requirements of the reflecting surface. Generally, the main strategies followed by LDR
 56 developers and designers is to use the tie system, connecting front and rear nets, to locally move
 57 single nodes. This operation is long and delicate but allows to adjust different error sources such as
 58 manufacturing errors [7–9], material definition errors, clearance [10,11], friction [12,13], hysteresis [14],
 59 mechanical vibrations [15,16], not perfect behaviour of elastic properties of components. This paper
 60 describes a method for the tie system calibration of LDRs with rigid or flexible ring truss. To our
 61 knowledge this topic has not been deeply investigated in the literature and the adjustment phase is
 62 entrusted with proprietary solutions of LDR companies. The outline of this paper is as follows. In
 63 Section 2 the problem of correcting the parameters to satisfy the static equilibrium in the deployed
 64 configuration is first addressed. Then, the method to find the necessary corrections to the tie-system
 65 is discussed for the two cases of LDR with rigid and flexible ring truss. In Section 3 the method
 66 is applied to a LDR with asymmetric ring truss developed by Thales Alenia Space. A simulated
 67 error distribution is superimposed to the design configuration to represent a real experimental test.
 68 Tie-system corrections, expressed in terms of length elongation or shortening, necessary to meet RMS
 69 design requirement are obtained for both rigid and flexible ring truss cases. Finally, conclusions close
 70 the paper.

71 2. Experimental setting for calibration

72 Once the antenna has been manufactured, it is necessary to carry out some experimental tests
 73 in order to check for the RMS of the reflector in the deployed configuration. To do this, the first
 74 operation consists of measuring the position of all nodes of the nets with respect to a reference system
 75 through one of the methods described in the Introduction. Due to different sources of errors such as
 76 manufacturing errors, assembly errors, the deployed configuration will be different from the design
 77 configuration and the RMS will be usually greater than the design requirement. Even the measurement

operation of the nodes coordinates will be affected by errors. Laser trackers and photogrammetry have errors on the order of $1 \mu\text{m}$; while laser radar reaches $0.1 \mu\text{m}$. Anyway, errors related to measurement systems maintain significantly below the proceeding mechanical errors. In the following, two methods for the experimental setting of the rigid and flexible ring truss support are described.

Several experimental methodologies [17–20] based on multibody approach have been developed [21–29]. Recently, methods based on the Fuzzy logic [30–34], neural networks [35] and genetic algorithm have been applied for the tensioning of space trusses [36,37]. The proposed methods act on the tensioning system of the ties to fix the errors coming from the construction of the antenna.

2.1. Rigid ring truss support: construction length determination

Tie cables regulation is usually independent from the actuators used for the LDA deployment [38–40] and from the control system [41–44]. Here, the method to regulate tie cables tension of an antenna with rigid ring truss support is first described. Once the deployment has been carried out and all node coordinates of the net have been measured the reflective surface deviated from the design configuration due to mechanical errors. As a consequence of this deviation, the system of equilibrium equation is not satisfied for the current configuration. Then, denoting with E_{ij} , A_{ij} , L_{ij} , L_{ij}^0 the Young modulus, the cross-section area, the measured length, the construction length of cable/tie ij , respectively and with k_{ij} the spring constant of tie ij , the system of nonlinear equations for each free node i , with j adjacent nodes, is not satisfied:

$$\begin{cases} \sum_j [E_{ij} A_{ij} \frac{L_{ij} - L_{ij}^0}{L_{ij}^0} + k_{ij} (L_{ij} - L_{ij}^0)] \frac{x_i - x_j}{L_{ij}} \neq 0 \\ \sum_j [E_{ij} A_{ij} \frac{L_{ij} - L_{ij}^0}{L_{ij}^0} + k_{ij} (L_{ij} - L_{ij}^0)] \frac{y_i - y_j}{L_{ij}} \neq 0 \\ \sum_j [E_{ij} A_{ij} \frac{L_{ij} - L_{ij}^0}{L_{ij}^0} + k_{ij} (L_{ij} - L_{ij}^0)] \frac{z_i - z_j}{L_{ij}} \neq 0 \end{cases} \quad (1)$$

where x_l , y_l and z_l are the measured Cartesian coordinates of the l -th node. It is noteworthy to remark that the only measured parameters are the node coordinates; while the *measured* length is derived using the Euclidian norm. The remaining parameters of the previous system are design parameters instead, each affected by different types of error. Here, we choose to gather all these errors inside the construction length L_{ij}^0 defined as the distance between the centers of the eyelets i and j belonging to the same cable, as shown in Fig. 4. This choice is motivated by the fact that the construction length of the cables is affected by two main sources of errors such as the *manufacturing errors*, generated during the cutting operation of CNC machines [45], and the *assembly errors*, coming from a bad placement of the eyelets necessary to connect two or more cables. In order to restore the equilibrium condition in system (1) only the design parameters can be adjusted while the measured parameters describe the real configuration of equilibrium: the measured configuration is already of equilibrium, thus system (1) is to be satisfied in this configuration without changing node coordinates.

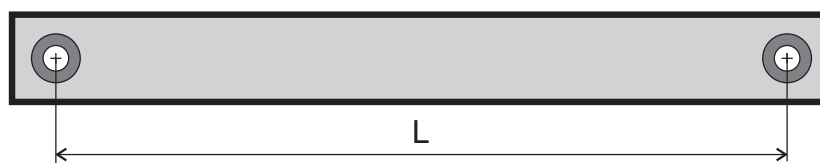


Figure 4. Layout of a cable: the construction length L_0 is affected by *manufacturing errors*, generated during the cutting operation and *assembly errors* coming from a bad placement of the eyelets necessary to connect two or more cables

Then, as each cable works in traction force only, the constraint $L_{ij} \geq L_{ij}^0$ must be imposed. To solve the system of nonlinear equation, Matlab[®] provides the command `fsolve`, but it does not allow to include any constraint. To overcome this problem it can be used the nonlinear programming solver

fmincon by giving a constant objective function and setting the eq.(1) as the nonlinear equality constraint, in addition to the linear inequality constraint $L_{ij} \geq L_{ij}^0$. The resulting constrained optimization problem is described below:

$$\begin{cases} \text{find } L_{ij}^0, \forall \text{cables and ties} \\ \text{min constant objective function} \\ \text{s.t. } L_{ij} \geq L_{ij}^0 \end{cases} \quad (2)$$

Hence, a first check is required. Because the springs used in tension ties require a prestress value, here denoted with F^0 , representing the minimum value necessary for their activation, the condition $F_{ij} \geq F_{ij}^0$ for each tension tie cable must be verified, where

$$F_{ij} = k_{ij}(L_{ij} - L_{ij}^0) \quad (3)$$

99 is the spring force of tie ij . If the condition is satisfied the next step can be conducted, otherwise the
100 spring belonging to the tie which has failed the test must be replaced and the algorithm starts again
101 calculating the array L^0 of all construction lengths.

102 2.2. Rear nodes determination

103 In the event that only the coordinates of the nodes of the front net are known by measurement,
104 before implementing the algorithm described above, the rear nodes coordinates have to be estimated.
105 Their coordinates are initialized with the design data and the system (1) for each free node of the front
106 and rear net is implemented. It can be noted the dualism between the two methods: in the former, the
107 unknowns are the construction lengths, in the latter the rear node coordinates. Then, the construction
108 lengths are obtained as a consequence using the Euclidian norm. We checked that both methods lead
109 to the same results, unless negligible errors, if the experimental configuration is not too distant from
110 the design one.

111 2.3. Rigid ring truss support: tie calibration

112 Once the configuration satisfying the static equilibrium has been found, the algorithm continues
113 with the estimation of the values of stretching or shortening for each tension tie cable that ensure that
114 the surface accuracy of the reflector can be met. The Figure 5 shows the screw adjustment system of a
115 tie. One fixed part is connected to a node of the front net while one mobile part, adjustable through a
116 screw, is connected to a node of the rear net. Now, the system of nonlinear equation of each free node i
117 can be written as follows:

$$\begin{cases} \sum_j [E_{ij} A_{ij} \frac{L_{ij} - L_{ij}^0}{L_{ij}^0} + k_{ij}(L_{ij} - L_{ij}^0 + \delta L_{ij})] \frac{x_i - x_j}{L_{ij}} = 0 \\ \sum_j [E_{ij} A_{ij} \frac{L_{ij} - L_{ij}^0}{L_{ij}^0} + k_{ij}(L_{ij} - L_{ij}^0 + \delta L_{ij})] \frac{y_i - y_j}{L_{ij}} = 0 \\ \sum_j [E_{ij} A_{ij} \frac{L_{ij} - L_{ij}^0}{L_{ij}^0} + k_{ij}(L_{ij} - L_{ij}^0 + \delta L_{ij})] \frac{z_i - z_j}{L_{ij}} = 0 \end{cases} \quad (4)$$

This system is similar to (1), used to determine the vector L^0 , with the difference that, this time, the variables to be found are the stretching/shortening values δL_{ij} and the coordinates of the free nodes of the front and rear net. The values δL_{ij} can be positive or negative: here we assume positive values for tie shortening and negative for tie stretching. Also this system is subject to some constraints. One condition for all net cables is that $L \geq L^0$. For the tension tie cables, for which the values δL_{ij} are to be considered, the constraint condition is that the final force F_{ij} must be of traction:

$$F_{ij} = k_{ij}(L_{ij} - L_{ij}^0) + k_{ij}\delta L_{ij} \geq 0 \Rightarrow L_{ij} + \delta L_{ij} \geq L_{ij}^0 \quad (5)$$

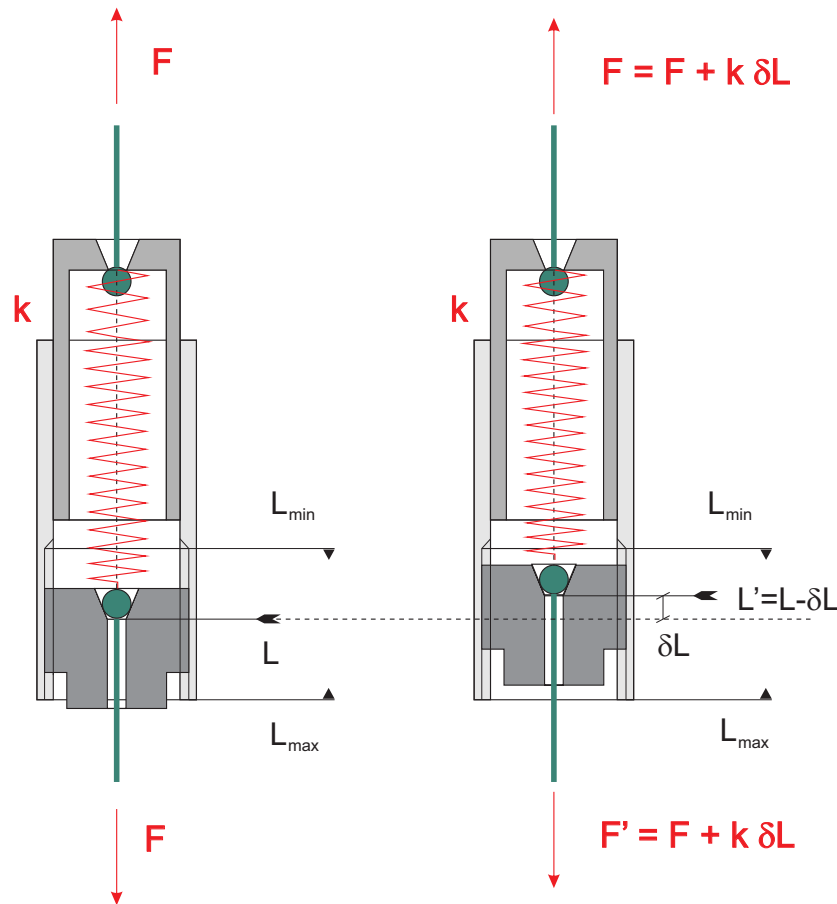


Figure 5. Screw adjustment tie system: (left) tie system before the adjustment; (right) tie system after the screw regulation.

118 Finally, the third constraint is related to the surface accuracy since the RMS error must be lower than
 119 the desired design value RMS_{target} . This is a typical constrained optimization problem largely used in
 120 design optimization of complex systems [46–49] and mechanisms [50–52]. The optimization problem
 121 can be summarised as follows:

$$\left\{ \begin{array}{ll} \text{find} & \mathbf{x}_1, \mathbf{y}_1, \mathbf{z}_1 \text{ and } \delta \mathbf{L} \\ \text{min} & \text{constant objective function} \\ \text{s. t.} & L_{ij} \geq L_{ij}^0 \quad \text{net cables} \\ & L_{ij} + \delta L_{ij} \geq L_{ij}^0 \quad \text{tension tie cables} \\ & RMS \leq RMS_{target} \quad \text{reflecting surface requirement} \end{array} \right. \quad (6)$$

122 where \mathbf{x}_1 , \mathbf{y}_1 and \mathbf{z}_1 are the free node coordinates and $\delta \mathbf{L}$ is the array containing all corrections δL_{ij} .
 123 The RMS is calculated by measuring the minimum distance of the free nodes of the front net compared
 124 to the ideal surface of the paraboloid (citazione primo articolo). The initial condition for the free nodes
 125 is represented by their experimental measurement, while the guess value for $\delta \mathbf{L}$ is set equal to zero.

126 2.4. Flexible ring truss support

127 The truss support is generally manufactured in carbon fiber and is therefore reasonable to consider
 128 the truss deformation under the effect of the tension of the cable net.

129 The elastodynamic model of the flexible ring truss support can be found using analytic techniques
 130 combined with the Matrix Structural Analysis, [53–56], elliptic integrals [57,58], FEM models [59–61],
 131 and flexible multibody formulations [62].

132 This implies the displacement of the nodes connected to the truss support, also called vertices,
 133 when the net system is tensioned. By considering the stiffness of the structure, the nonlinear system (4)
 134 described in the previous section becomes as follows:

$$\left\{ \begin{array}{l} \left[\sum_{j=1}^{c-r} E_{ij} A_{ij} \frac{L_{ij} - L_{ij}^0}{L_{ij}^0} + \sum_{j=1}^r (E_{ij} A_{ij} \frac{L_{ij} - L_{ij}^0}{L_{ij}^0} - k_{xx_{ij}} (x_{v_j} - x_{v_j}^0)) \right. \\ \quad \left. + k_{ij} (L_{ij} - L_{ij}^0 + \delta L_{ij}) \right] \frac{x_i - x_j}{L_{ij}} = 0 \\ \left[\sum_{j=1}^{c-r} E_{ij} A_{ij} \frac{L_{ij} - L_{ij}^0}{L_{ij}^0} + \sum_{j=1}^r (E_{ij} A_{ij} \frac{L_{ij} - L_{ij}^0}{L_{ij}^0} - k_{yy_{ij}} (y_{v_j} - y_{v_j}^0)) \right. \\ \quad \left. + k_{ij} (L_{ij} - L_{ij}^0 + \delta L_{ij}) \right] \frac{y_i - y_j}{L_{ij}} = 0 \\ \left[\sum_{j=1}^{c-r} E_{ij} A_{ij} \frac{L_{ij} - L_{ij}^0}{L_{ij}^0} + \sum_{j=1}^r (E_{ij} A_{ij} \frac{L_{ij} - L_{ij}^0}{L_{ij}^0} - k_{zz_{ij}} (z_{v_j} - z_{v_j}^0)) \right. \\ \quad \left. + k_{ij} (L_{ij} - L_{ij}^0 + \delta L_{ij}) \right] \frac{z_i - z_j}{L_{ij}} = 0 \end{array} \right. \quad (7)$$

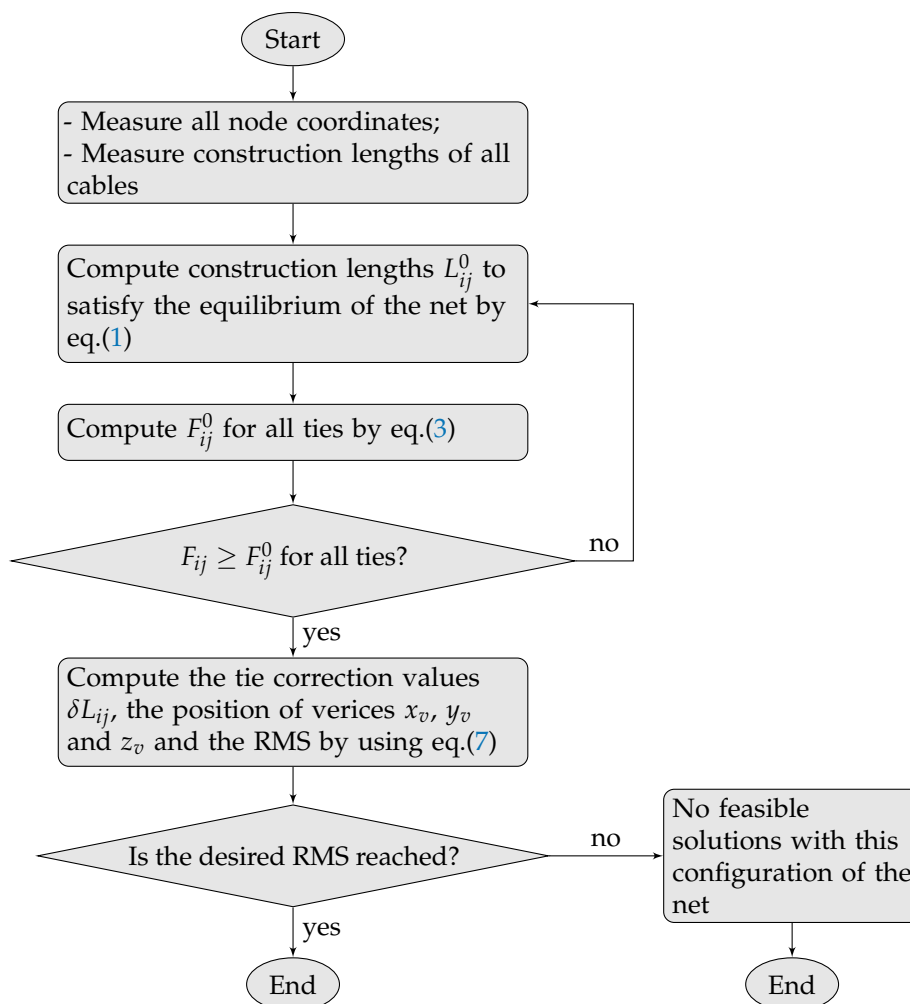


Figure 6. Algorithm of the method

135

136 where c is the total number of cables connected to the i -th node; r is the number of rods, x_v, y_v
 137 and z_v are the unknown coordinates of the j -th vertex and x_v^0, y_v^0 and z_v^0 the initial coordinates of the

138 vertex itself. The stiffness of the truss support can be represented as a three-dimensional bushing, with
 139 stiffnesses k_{xxij} , k_{yyij} and k_{zzij} , connecting the rods to the vertex, as shown in Fig. 7. The constrained
 140 optimization (6) still applies to this flexible ring truss case and the overall algorithm is summarised in
 141 the flowchart of Fig. 6.

142 3. Results

143 In order to verify the validity of the proposed method, the case study of an asymmetric large
 144 deployable reflector, designed by Thales Alenia Space [63], is described. Relevant parameters and
 145 geometrical data are listed as follows:

- 146 • Focal length: 6 (m)
- 147 • Number of free nodes: 296
- 148 • Number of vertices: 14
- 149 • Number of total cables: 1044
- 150 • Cable section: 4 (mm)^2
- 151 • Young modulus of cables: $8.3 \times 10^{10} \text{ (N/m)}^2$
- 152 • Initial RMS error: 0.5872 (mm)
- 153 • Design value of the RMS faceting error: 0.21 (mm)

154 The value of spring constant in tie cables ranges from $2 \times 10^3 \text{ N/m}$ to $68 \times 10^3 \text{ N/m}$ with radial
 155 step of $11 \times 10^3 \text{ N/m}$ starting from the centre (central node) to the outer ring cables. The initial RMS
 156 error on the front net was simulated by introducing an additional value to each node proportionally to

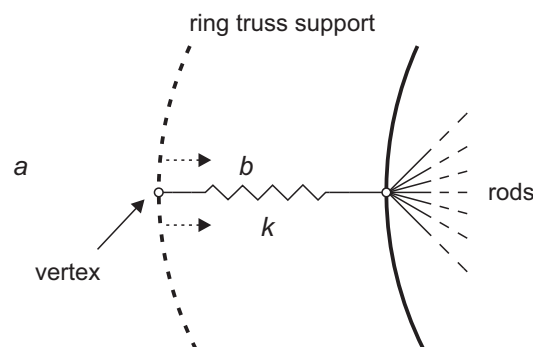


Figure 7. Displacement of the vertex due to the deformation of the flexible ring truss support

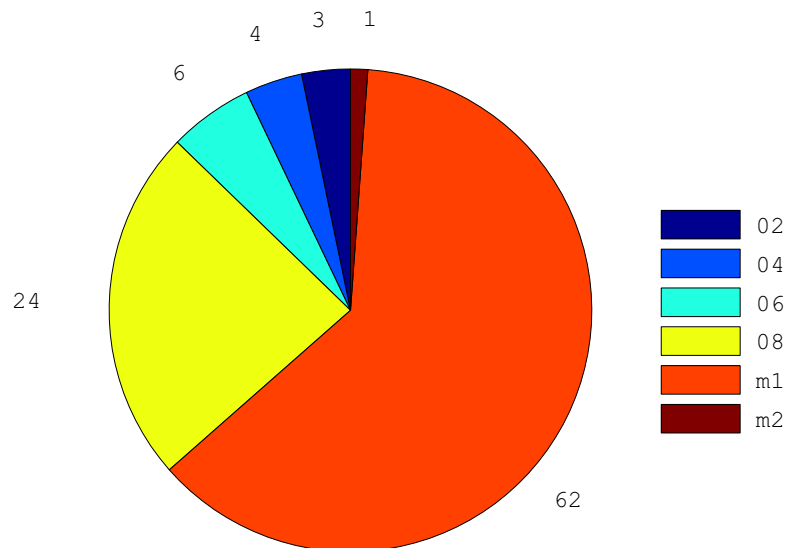


Figure 8. Pie chart of the error (absolute value), grouped by measuring ranges (mm), between the measured construction lengths and those obtained by solving equilibrium in system (1).

157 the length of the tie connected to it. By imposing the equilibrium in the system (1) we can determine the
 158 construction lengths described in Section 2. Nevertheless, from Fig. 8 it can be noted that the maximum
 159 error e_{L0} obtained is about 1 (mm), representing only 1% of total cables; the largest percentage (86%)
 showing an error between 0.6 (mm) and 1 (mm).

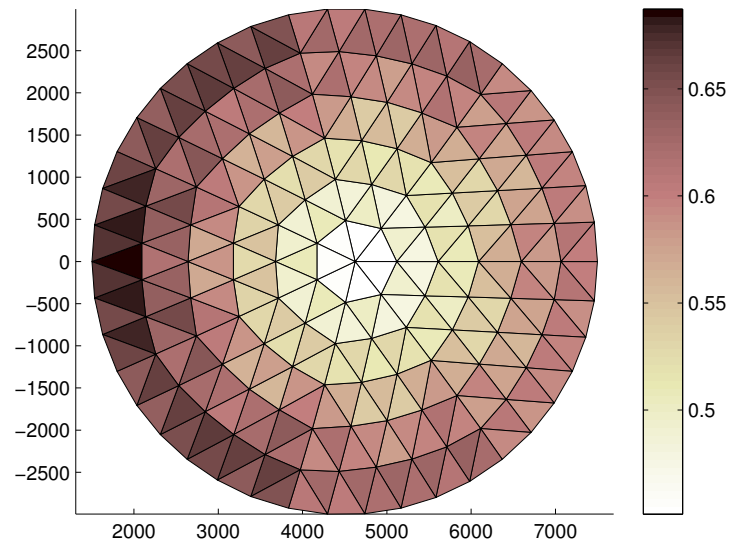


Figure 9. Faceted RMS (mm) of the front tension truss in the initial configuration.

160
 161 In Fig. 9 the local faceting error for the chosen initial configuration is shown. The local faceting
 162 error is calculated considering the centroid of the triangular facets in which the surface can be
 163 decomposed [64–67]. As it can be observed, the faceting error follows the shape of the asymmetric
 164 reflector because the chosen error is proportional to the tie lengths. As a matter of fact, the central zone
 165 is the one with the shortest cables and therefore with the lowest faceting error. On the contrary, the tie
 166 lengths, and consequently the errors, grow moving from the centre to the outer perimeter of the net.

167 The optimization method described in the previous sections is first applied to the rigid ring truss
 168 support. The Figure 10 shows the error of each free node of the front net with respect to the ideal
 169 surface coupled with the stretching/shortening value necessary to reach the desired surface accuracy.
 170 The reason why correction values are all positive is that the initial error is simulated by positioning all
 171 nodes of the front net above the ideal surface, so there is the need to shorten the tie lengths to satisfy
 172 the RMS design value. The bars are grouped by spring constant value.

173 The corresponding faceting error is shown in Fig. 11. As it can be observed the RMS of the faceting
 174 error is lowered till the required value of 0.2036 (mm) furnished as specification.

175 Then, the same analysis has been performed for the flexible ring truss support. It can be noted that
 176 in the Fig. 12, the correction values are lower than the corresponding values with rigid truss support:
 177 this is because the additional tensioning of ties further deforms the shape of the truss support resulting
 178 in a closure of the support itself [68]. As a result, this causes a slight lowering of the front net thus
 179 reducing the shortening action of tie lengths. Finally, the Fig. 13 shows the faceting error distribution
 180 on the front net. Even in this case the final RMS faceting error reached 0.2045 (mm) representing
 181 the design value of the RMS. Comparing the two Figs. 11 and 13 it can be observed that the faceting
 182 error distribution is more uniform for the flexible ring truss support. This result can be explained
 183 considering that the deformation of the truss support relaxes the front and rear tension truss systems
 184 making the tension distribution more uniform.

185 Moreover, other simulations with different initial RMS errors revealed that, with the given design
 186 data, the maximum initial RMS error which can be fixed is about 1 (mm). Beyond this limit value, a

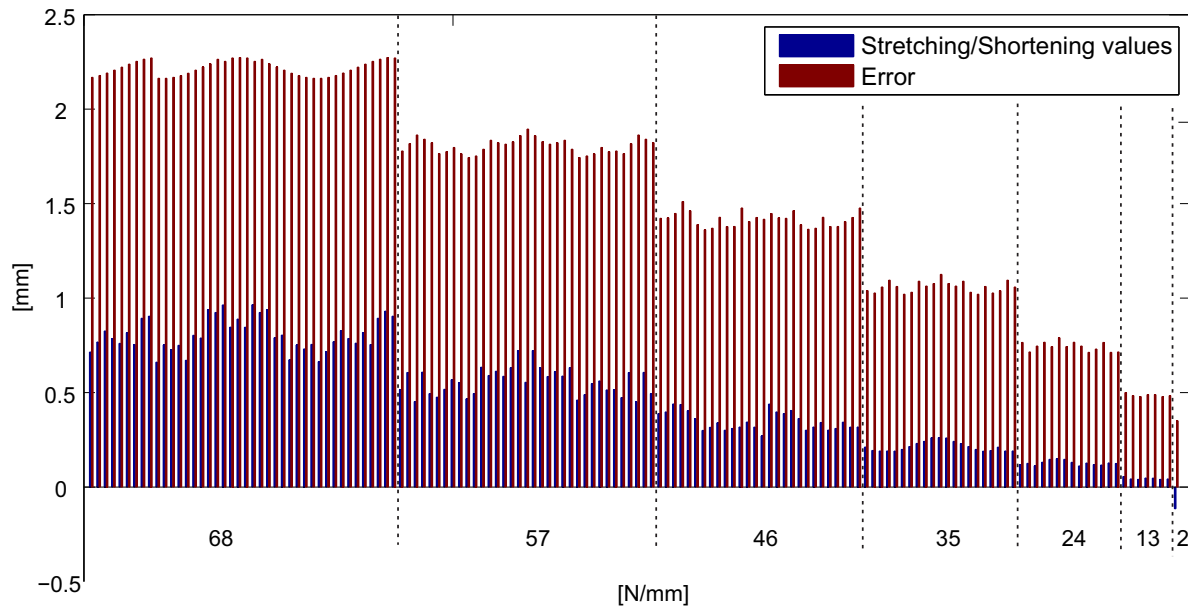


Figure 10. Error and correction values (rigid case)

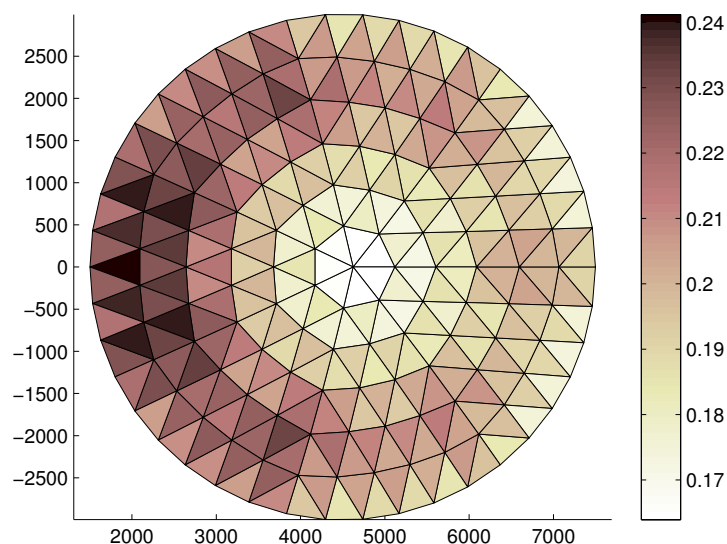


Figure 11. Faceting error (mm) distribution on the front tension truss obtained for the rigid ring truss support

187 revision of design data is needed. This demonstrates the validity of the method only for small RMS
188 errors.

189 4. Conclusions

190 In this paper a method for the tie-system calibration of Large Deployable Reflectors (LDRs) is
191 provided. The LDRs are very sensitive to errors and usually require a careful experimental setup to
192 meet the design requirement of surface accuracy. Due to manufacturing errors, clearance, friction, not
193 perfect behaviour of materials the real configuration moves away from the design configuration and a
194 fine calibration is needed to improve the quality of the reflecting surface expressed in terms of closeness
195 to the ideal paraboloidal geometry. The proposed method follows two steps: the determination of the
196 parameters satisfying the static equilibrium in the real deployed configuration; the fine calibration

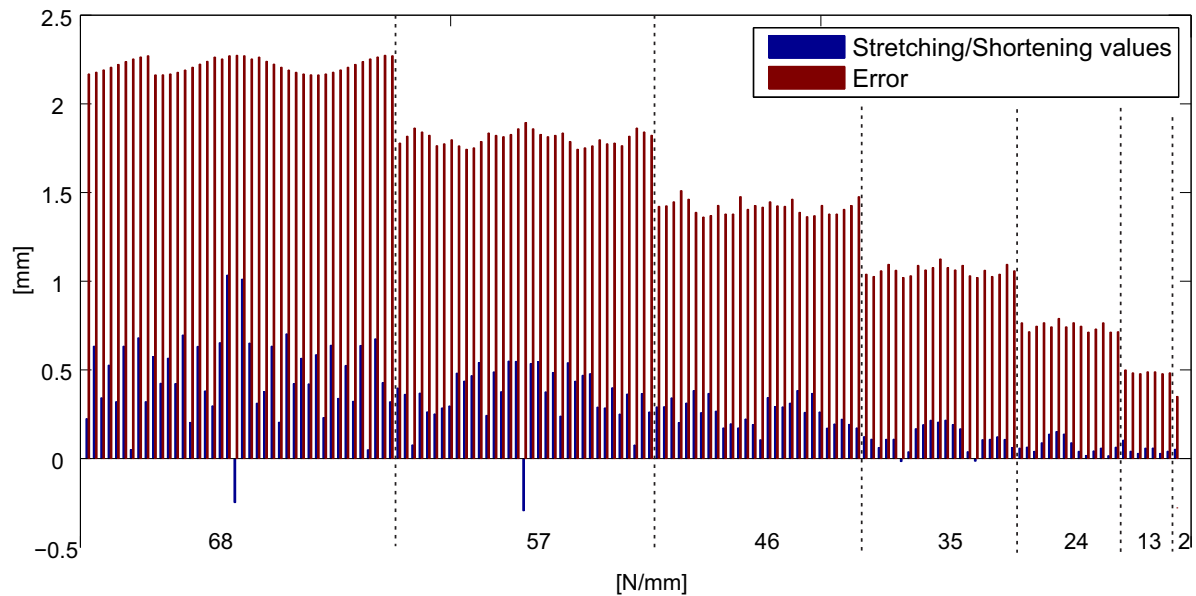


Figure 12. Error and correction values (flexible case)

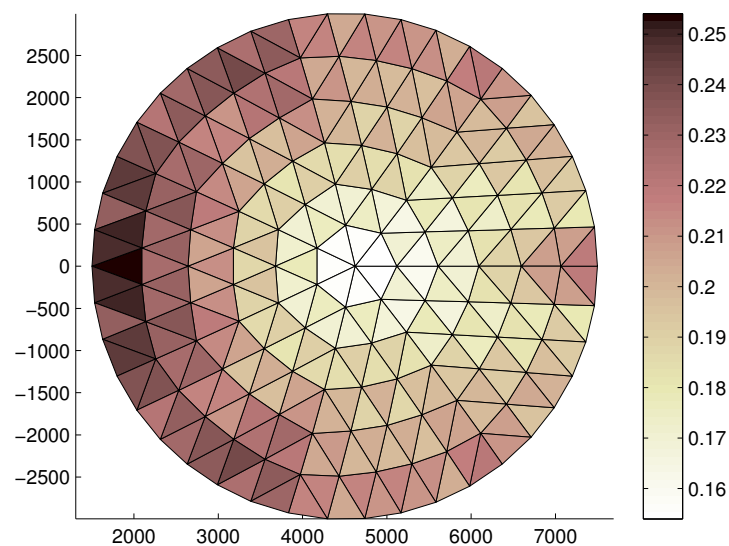


Figure 13. Faceting error (mm) distribution on the front tension truss obtained for the flexible ring truss support

197 to meet RMS design requirements. For the first step a constrained optimization problem has been
 198 proposed to find the cable construction lengths once all node coordinates have been measured. The
 199 second step has been developed acting on the system of screw adjustable ties. A further constrained
 200 optimization problem has been formulated to find the length corrections of each tie. Using the same
 201 approach the cases of LDR with rigid and flexible tension truss have been studied. Finally, the method
 202 has been applied to a LDR with asymmetrical ring truss designed by Thales Alenia Space. Considering
 203 an initial RMS of 0.58 (mm) the results, not yet validated by experimental test, seemed comforting in
 204 reaching the design RMS. The method convergency depends on the starting and desired RMS. Here,
 205 the convergency has been insured up to the reasonable high initial RMS value of 1 (mm): beyond this
 206 value the tie system is not able to reach the equilibrium and satisfy the constraints and a different
 207 solution should be adopted.

208 **Author Contributions:** This research paper was principally developed by the first and last author (A.C. and
209 P.D.M.). The other two authors (R.S. and R.R.) have dealt with the significant review activity.

210 **Funding:** “This research was funded by ESA grant number AO/1-7217/NL/CP - Innovative Scalable Large
211 Deployable Antenna Reflectors.”

212 **Acknowledgments:** This work has been partially financed by the University of Catania within the project “Piano
213 della Ricerca Dipartimentale 2016-2018” of the Department of Civil Engineering and Architecture.

214 **Conflicts of Interest:** “The authors declare no conflict of interest.”

215 Abbreviations

216 The following abbreviations are used in this manuscript:

217	MDPI	Multidisciplinary Digital Publishing Institute
	DOAJ	Directory of open access journals
218	TLA	Three letter acronym
	LD	linear dichroism

219 References

- 220 1. Thomson, M. AstroMesh™ deployable reflectors for ku and ka band commercial satellites. 20th AIAA
221 international communication satellite systems conference and exhibit, 2002, p. 2032.
- 222 2. Estler, W.T.; Edmundson, K.; Peggs, G.; Parker, D. Large-scale metrology—an update. *CIRP*
223 *Annals-Manufacturing Technology* **2002**, *51*, 587–609.
- 224 3. De Simone, M.C.; Guida, D. On the Development of a Low Cost Device for Retrofitting Tracked Vehicles
225 for Autonomous Navigation. *Proceedings of the AIMETA* **2017**.
- 226 4. Cuypers, W.; Van Gestel, N.; Voet, A.; Kruth, J.P.; Mingneau, J.; Bleys, P. Optical measurement techniques
227 for mobile and large-scale dimensional metrology. *Optics and Lasers in Engineering* **2009**, *47*, 292–300.
- 228 5. Dong, M.L.; Deng, W.Y.; Sun, Y.; Wang, Y. Photogrammetric Measurement of Deformation of Large
229 Deployable Mesh Microwave Antenna. *Key Engineering Materials*. Trans Tech Publ, 2008, Vol. 381, pp.
230 309–312.
- 231 6. Stegman, M.D.; Fedyk, M.; Kuehn, S. Solar thermal vacuum testing of deployable mesh reflector for model
232 correlation. *Aerospace Conference, 2010 IEEE*. IEEE, 2010, pp. 1–15.
- 233 7. Zhang, Y.; Li, Z.; Gao, J.; Hong, J.; Vilecco, F.; Li, Y. A method for designing assembly tolerance networks
234 of mechanical assemblies. *Mathematical Problems in Engineering* **2012**, 2012.
- 235 8. Vilecco, F.; Pellegrino, A. Evaluation of uncertainties in the design process of complex mechanical systems.
236 *Entropy* **2017**, *19*, 475.
- 237 9. Vilecco, F. On the evaluation of errors in the virtual design of mechanical systems. *Machines* **2018**, *6*, 36.
- 238 10. Cammarata, A.; Lacagnina, M.; Sinatra, R. Closed-form solutions for the inverse kinematics of the Agile
239 Eye with constraint errors on the revolute joint axes. *Intelligent Robots and Systems (IROS), 2016 IEEE/RSJ*
240 *International Conference on*. IEEE, 2016, pp. 317–322.
- 241 11. Cammarata, A. A novel method to determine position and orientation errors in clearance-affected
242 overconstrained mechanisms. *Mechanism and Machine Theory* **2017**, *118*, 247–264.
- 243 12. De Simone, M.; Guida, D. Dry friction influence on structure dynamics. *Proceedings of the COMPDYN* **2015**.
- 244 13. De Simone, M.C.; Guida, D. Modal Coupling in Presence of Dry Friction. *Machines* **2018**, *6*, 8.
- 245 14. Guida, D.; Pappalardo, C.M. Control design of an active suspension system for a quarter-car model with
246 hysteresis. *JOURNAL OF VIBRATION ENGINEERING & TECHNOLOGIES* **2015**, *3*, 277–299.
- 247 15. Pappalardo, C.M.; Guida, D. Adjoint-based optimization procedure for active vibration control of nonlinear
248 mechanical systems. *Journal of Dynamic Systems, Measurement, and Control* **2017**, *139*, 081010.
- 249 16. Pappalardo, C.M.; Guida, D. Control of nonlinear vibrations using the adjoint method. *Meccanica* **2017**,
250 *52*, 2503–2526.
- 251 17. Pappalardo, C.M.; Guida, D. A time-domain system identification numerical procedure for obtaining linear
252 dynamical models of multibody mechanical systems. *Archive of Applied Mechanics* **2018**, *88*, 1325–1347.
- 253 18. Pappalardo, C.M.; Guida, D. On the use of two-dimensional Euler parameters for the dynamic simulation
254 of planar rigid multibody systems. *Archive of Applied Mechanics* **2017**, *87*, 1647–1665.

- 255 19. Pappalardo, C.M.; Guida, D. System Identification Algorithm for Computing the Modal Parameters of
256 Linear Mechanical Systems. *Machines* **2018**, *6*, 12.
- 257 20. Pappalardo, C.M.; Guida, D. System Identification and Experimental Modal Analysis of a Frame Structure.
258 *Engineering Letters* **2018**, *26*.
- 259 21. Cavacece, M.; Pennestri, E.; Sinatra, R. Experiences in teaching multibody dynamics. *Multibody System
260 Dynamics* **2005**, *13*, 363–369.
- 261 22. Callegari, M.; Cammarata, A.; Gabrielli, A.; Sinatra, R. Kinematics and dynamics of a 3-CRU spherical
262 parallel robot. ASME 2007 International Design Engineering Technical Conferences and Computers and
263 Information in Engineering Conference. American Society of Mechanical Engineers, 2007, pp. 933–941.
- 264 23. Cammarata, A.; Angeles, J.; Sinatra, R. Kinetostatic and inertial conditioning of the McGill
265 Schönflies-motion generator. *Advances in Mechanical Engineering* **2010**, *2*, 186203.
- 266 24. Barbagallo, R.; Sequenzia, G.; Oliveri, S.; Cammarata, A. Dynamics of a high-performance motorcycle by
267 an advanced multibody/control co-simulation. *Proceedings of the Institution of Mechanical Engineers, Part K:
268 Journal of Multi-body Dynamics* **2016**, *230*, 207–221.
- 269 25. Barbagallo, R.; Sequenzia, G.; Cammarata, A.; Oliveri, S.; Fatuzzo, G. Redesign and multibody simulation
270 of a motorcycle rear suspension with eccentric mechanism. *International Journal on Interactive Design and
271 Manufacturing (IJIDeM)* **2017**, pp. 1–8.
- 272 26. De Simone, M.C.; Russo, S.; Rivera, Z.B.; Guida, D. Multibody model of a UAV in presence of wind fields.
273 Control, Artificial Intelligence, Robotics & Optimization (ICCAIRO), 2017 International Conference on.
274 IEEE, 2017, pp. 83–88.
- 275 27. Pappalardo, C.M.; Guida, D. Dynamic analysis of planar rigid multibody systems modeled using natural
276 absolute coordinates. *Applied and Computational Mechanics* **2018**, *12*.
- 277 28. Pappalardo, C.M.; Guida, D. On the Lagrange multipliers of the intrinsic constraint equations of rigid
278 multibody mechanical systems. *Archive of Applied Mechanics* **2018**, *88*, 419–451.
- 279 29. Pappalardo, C.M.; Guida, D. On the Computational Methods for Solving the Differential-Algebraic
280 Equations of Motion of Multibody Systems. *Machines* **2018**, *6*, 20.
- 281 30. Ghomshei, M.; Vilecco, F.; Porkhial, S.; Pappalardo, M. Complexity in energy policy: A fuzzy logic
282 methodology. Fuzzy Systems and Knowledge Discovery, 2009. FSKD'09. Sixth International Conference
283 on. IEEE, 2009, Vol. 7, pp. 128–131.
- 284 31. Ghomshei, M.; Vilecco, F. Energy metrics and Sustainability. International Conference on Computational
285 Science and Its Applications. Springer, 2009, pp. 693–698.
- 286 32. Sena, P.; Attianese, P.; Carbone, F.; Pellegrino, A.; Pinto, A.; Vilecco, F. A fuzzy model to interpret data
287 of drive performances from patients with sleep deprivation. *Computational and mathematical methods in
288 medicine* **2012**, *2012*.
- 289 33. Sena, P.; d'Amore, M.; Pappalardo, M.; Pellegrino, A.; Fiorentino, A.; Vilecco, F. Studying the influence of
290 cognitive load on driver's performances by a Fuzzy analysis of Lane Keeping in a drive simulation. *IFAC
291 Proceedings Volumes* **2013**, *46*, 151–156.
- 292 34. Sena, P.; Attianese, P.; Pappalardo, M.; Vilecco, F. FIDELITY: Fuzzy inferential diagnostic engine for on-line
293 support to physicians. 4th International Conference on Biomedical Engineering in Vietnam. Springer, 2013,
294 pp. 396–400.
- 295 35. Object Recognition by Using Neural Networks For Robotics Precision Agriculture Application, author=De
296 Simone, Marco Claudio and Guida, Domenico, journal=Engineering Letters, year=2018, publisher=under
297 review.
- 298 36. Salajegheh, E.; Salajegheh, J.; SEYEDPOUR, S.; Khatibinia, M. Optimal design of geometrically nonlinear
299 space trusses using an adaptive neuro-fuzzy inference system **2009**.
- 300 37. Finotto, V.C.; da Silva, W.R.; Valášek, M.; Štemberk, P. Hybrid fuzzy-genetic system for optimising
301 cabled-truss structures. *Advances in Engineering Software* **2013**, *62*, 85–96.
- 302 38. Pirrotta, S.; Sinatra, R.; Meschini, A. A novel simulation model for ring type ultrasonic motor. *Meccanica*
303 **2007**, *42*, 127–139.
- 304 39. De Simone, M.C.; Rivera, Z.B.; Guida, D. Obstacle Avoidance System for Unmanned Ground Vehicles by
305 Using Ultrasonic Sensors. *Machines* **2018**, *6*, 18.
- 306 40. Iannone, V.; De Simone, M.C. Modelling of a DC Gear Motor for Feed-Forward Control Law Design for
307 Unmanned Ground Vehicles. *Actuators* **2018**.

- 308 41. Zhai, Y.; Liu, L.; Lu, W.; Li, Y.; Yang, S.; Vilecco, F. The application of disturbance observer to propulsion
309 control of sub-mini underwater robot. *International Conference on Computational Science and Its*
310 *Applications*. Springer, 2010, pp. 590–598.
- 311 42. De, S.; Rivera, Z.; Guida, D.; others. A new semi-active suspension system for racing vehicles. *FME*
312 *Transactions* **2017**, *45*, 578–584.
- 313 43. De Simone, M.C.; Guida, D. Identification and Control of a Unmanned Ground Vehicle By using Arduino.
314 *UIPB Sci. Bull. Ser. D* **2018**, *80*, 141–154.
- 315 44. De, S.; Guida, D. Control design for an under-actuated UAV model. *FME Transactions* **2018**, *46*, 443–452.
- 316 45. Quatrano, A.; De, S.; Rivera, Z.; Guida, D. Development and implementation of a control system for a
317 retrofitted CNC machine by using Arduino. *FME Transactions* **2017**, *45*, 565–571.
- 318 46. Pellegrino, A.; Vilecco, F. Design optimization of a natural gas substation with intensification of the energy
319 cycle. *Mathematical Problems in Engineering* **2010**, 2010.
- 320 47. Formato, A.; Ianniello, D.; Vilecco, F.; Lenza, T.L.L.; Guida, D. Design optimization of the plough working
321 surface by computerized mathematical model. *Emirates Journal of Food and Agriculture* **2017**, pp. 36–44.
- 322 48. Formato, A.; Guida, D.; Ianniello, D.; Vilecco, F.; Lenza, T.; Pellegrino, A. Design of Delivery Valve for
323 Hydraulic Pumps. *Machines* **2018**, *6*, 44.
- 324 49. Muscat, M.; Cammarata, A.; Maddio, P.D.; Sinatra, R. Design and development of a towfish to monitor
325 marine pollution. *Euro-Mediterranean Journal for Environmental Integration* **2018**, *3*, 11.
- 326 50. Cammarata, A. Optimized design of a large-workspace 2-DOF parallel robot for solar tracking systems.
327 *Mechanism and machine theory* **2015**, *83*, 175–186.
- 328 51. Sequenzia, G.; Fatuzzo, G.; Oliveri, S.; Barbagallo, R. Interactive re-design of a novel variable geometry
329 bicycle saddle to prevent neurological pathologies. *International Journal on Interactive Design and*
330 *Manufacturing (IJIDeM)* **2016**, *10*, 165–172.
- 331 52. Barbagallo, R.; Sequenzia, G.; Cammarata, A.; Oliveri, S. An integrated approach to design an innovative
332 motorcycle rear suspension with eccentric mechanism. In *Advances on Mechanics, Design Engineering and*
333 *Manufacturing*; Springer, 2017; pp. 609–619.
- 334 53. Cammarata, A.; Sinatra, R. On the elastostatics of spherical parallel machines with curved links. In *Recent*
335 *Advances in Mechanism Design for Robotics*; Springer, 2015; pp. 347–356.
- 336 54. Cammarata, A.; Calì, I.; Greco, A.; Lacagnina, M.; Fichera, G.; others. Dynamic stiffness model of
337 spherical parallel robots. *Journal of Sound and Vibration* **2016**, *384*, 312–324.
- 338 55. Cammarata, A. Unified formulation for the stiffness analysis of spatial mechanisms. *Mechanism and*
339 *Machine Theory* **2016**, *105*, 272–284.
- 340 56. Cammarata, A.; Sinatra, R.; Maddio, P. A Two-Step Algorithm for the Dynamic Reduction of Flexible
341 Mechanisms. *IFTToMM Symposium on Mechanism Design for Robotics*. Springer, 2018, pp. 25–32.
- 342 57. Cammarata, A.; Sequenzia, G.; Oliveri, S.M.; Fatuzzo, G. Modified chain algorithm to study planar
343 compliant mechanisms. *International Journal on Interactive Design and Manufacturing (IJIDeM)* **2016**,
344 *10*, 191–201.
- 345 58. Cammarata, A.; Lacagnina, M.; Sequenzia, G. Alternative elliptic integral solution to the beam deflection
346 equations for the design of compliant mechanisms. *International Journal on Interactive Design and*
347 *Manufacturing (IJIDeM)* **2018**, pp. 1–7.
- 348 59. De, S.M.C.; Rivera, Z.; Guida, D. Finite element analysis on squeal-noise in railway applications. *FME*
349 *Transactions* **2018**, *46*, 93–100.
- 350 60. Oliveri, S.; Sequenzia, G.; Calì, M. Flexible multibody model of desmodromic timing system. *Mechanics*
351 *based design of structures and machines* **2009**, *37*, 15–30.
- 352 61. Calì, M.; Oliveri, S.M.; Sequenzia, G. Geometric modeling and modal stress formulation for flexible
353 multi-body dynamic analysis of crankshaft. 25th Conference and Exposition on Structural Dynamics, 2007,
354 pp. 1–9.
- 355 62. Pappalardo, C.M. A natural absolute coordinate formulation for the kinematic and dynamic analysis of
356 rigid multibody systems. *Nonlinear Dynamics* **2015**, *81*, 1841–1869.
- 357 63. Maddio, P.; Meschini, A.; Sinatra, R.; Cammarata, A. An optimized form-finding method of an asymmetric
358 large deployable reflector. *Engineering Structures* **2019**, *181*, 27–34.
- 359 64. Agrawal, P.; Anderson, M.; Card, M. Preliminary design of large reflectors with flat facets. *IEEE transactions*
360 *on antennas and propagation* **1981**, *29*, 688–694.

- 361 65. Li, P.; Liu, C.; Tian, Q.; Hu, H.; Song, Y. Dynamics of a deployable mesh reflector of satellite antenna:
362 form-finding and modal analysis. *Journal of Computational and Nonlinear Dynamics* **2016**, *11*, 041017.
- 363 66. Yuan, S.; Yang, B.; Fang, H. Improvement of Surface Accuracy for Large Deployable Mesh Reflectors.
364 AIAA/AAS Astrodynamics Specialist Conference, 2016, p. 5571.
- 365 67. Morterolle, S.; Maurin, B.; Quirant, J.; Dupuy, C. Numerical form-finding of geotensoid tension truss for
366 mesh reflector. *Acta Astronautica* **2012**, *76*, 154–163.
- 367 68. Liu, W.; Li, D.X.; Yu, X.Z.; Jiang, J.P. Exact mesh shape design of large cable-network antenna reflectors
368 with flexible ring truss supports. *Acta Mechanica Sinica* **2014**, *30*, 198–205.